Three-dimensional modelling of bond behaviour between concrete and FRP reinforcement

G. Mazzucco, V. Salomoni, C. Majorana, C. Pellegrino
Department of Structural and Transportation Engineering, University of Padua, Italy
E-mail: mazzucco@dic.unipd.it, salomoni@dic.unipd.it, majorana@dic.unipd.it, carlo.pellegrino@unipd.it

Keywords: Debonding, Damage Mechanics, FRP reinforcements.

SUMMARY. The bond behaviour between FRP and concrete elements is investigated, starting from available experimental evidences, through a calibrated and upgraded 3D mathematical-numerical model. The complex mechanism of debonding failure of FRP concrete reinforcement is studied within the context of damage mechanics to appropriately describe transversal effects and developing a realistic study of the delamination process.

1 INTRODUCTION

In these years the interest for FRP (Fiber Reinforced Polymers) applications in civil engineering structures is grown thanks to a series of aspects: fast and easy application of the fibers, low cost of interventions, etc. Externally bonded FRP sheets are currently used to repair and strengthen existing RC structures for shear [1, 2, 3] and flexural [4] applications. A problem of such a technique is the brittle fracture mechanism, depending on e.g. load level, concrete characteristics and rigidity of adhesive and FRP plate. Many experimental and analytical studies have been undertaken to understand the bond behaviour between FRP and substrate (e.g. [1, 5, 6]), and its current comprehension is generally related to semi-empirical 2D approaches. However two-dimensional interface models based on fracture and contact mechanics and on the evaluation of the energy release rate [7] describe well delamination mechanisms.

The present work proposes to investigate the bond behaviour between FRP and concrete elements, starting from already available experimental evidences to appropriately calibrate the mathematical - numerical model chosen for the simulation of the above phenomena, within a 3D domain. In this way transversal effects can be described allowing for a realistic and comprehensive study of the delamination process. Particularly, it is here proposed to study the complex mechanism of debonding failure of FRP reinforcements within the context of damage mechanics, appropriately enhancing the potentialities of the F.E. code ABAQUS, which allows for developing geometric non-linear and changing-status analyses, by supplementing it with a numerical procedure accounting for a scalar damage law inside the contact algorithm. It will be shown that such an approach is able to catch delamination and its evolution during the loading process by means of the comparison between numerical and experimental results [8].

2 NUMERICAL MODELLING OF DELAMINATION PROCESSES

A realistic numerical modeling of debonding within the FE context requires to implement damage laws in the contact conditions, being the contact algorithm alone not sufficient to catch the triggering of delamination and its evolution. Indeed the contact method is characterized by the conditions of contact or no-contact but the behaviour in the transition state is generally treated with a Coulomb friction procedure, hence getting a softening response is not possible. Again, the necessity of developing an upgraded contact procedure to model bonding-debonding processes is supported by

experimental evidences, as reported in the following. Delamination normally affects a thin layer of concrete, as the adhesive strength is typically much higher than the concrete tensile strength. Hence concrete cracking usually occurs in the superficial zone close to the interface only: this cracking due to debonding has been taken into account in the numerical model by means of the contact-damage model at the interface.

2.1 *Contact conditions*

The interaction between concrete and FRP can be represented through three steps. In the first step the shear stress at the interface is lower than the shear strength, and the FRP sheet (body A) is bonded with concrete (body B). Hence the contact surface is defined by:

$$\Gamma^C = \Gamma^A \bigcap \Gamma^B \tag{1}$$

with maximum dimension $\Gamma^C = \Gamma^C_{max}$. The second step starts when the shear strength is reached and slip occurs. Stresses approach zero following the softening curve produced by applying Mazars' damage model (see below). The contact surface is variable $0 < \Gamma^C < \Gamma^C_{max}$. The third step is characterized by complete debonding and $\Gamma^C = 0$.

2.2 *Mazars' law*

An isotropic damage law is here considered, based on the definition of a scalar variable D.

When $D = 0$ the material is virgin whereas, when $0 < D < 1$, the material is affected by damage, up to $D = 1$ corresponding to complete damage, i.e. fracture.

The evolution of damage $D = D(\widetilde{\epsilon})$ according to Mazars depends on the strain level and it is defined by

$$D = \begin{cases} 0 & \text{if } \widetilde{\epsilon} \leq \epsilon_0, \\ 1 - \frac{(1-A)K_0}{\widetilde{\epsilon}} - \frac{A}{e^{(B(\widetilde{\epsilon}-k_0))}} & \text{if } \widetilde{\epsilon} > \epsilon_0 \end{cases} \tag{2}$$

where A and B are material coefficients, ϵ_0 is the limit linear elastic strain, $(\widetilde{\epsilon})$ the equivalent strain and K_0 the initial value of the softening parameter. The reader is referred to [9, 10] for additional details. A 1D scheme for the proposed approach (applied to any direction) is shown in (Figure 1), where the elastic-damage feature of the model is referred to the adhesive layer, serving as the effective contact layer. Hence, the spring is elastic until a deformation limit ϵ_0 is reached and $D = 0$, then $\epsilon > \epsilon_0$ and damage becomes different from zero.

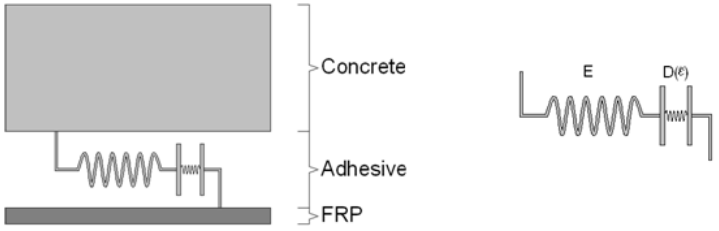

Figure 1: Left: Bonding scheme. Right: The analogical model for the elastic-damage law included in the contact algorithm.

The contact-damage model has been implemented using a fortran routine and linked to ABAQUS; the subroutine determines the 3D damage at each step and allows for the occurrence of sliding between the contact elements if D is different from zero.

2.3 Concrete constitutive law

A Drucker-Prager constitutive law has been assumed to model the non-linear behaviour of concrete in compression and tension, which is computationally efficient and whose results are not dependent on the mesh characteristics. The failure surface in the (t, p) plane is described by

$$F = t - p\tan\beta - d = 0 \tag{3}$$

where t is the deviatoric stress, β the friction angle, d the cohesion and p the hydrostatic stress component.

3 AVAILABLE EXPERIMENTAL DATA AND NUMERICAL ANALYSES

The experimental results used to validate the numerical model and check its effectiveness have already been published in [8] and are briefly recalled here for reasons of clarity. Effective bond length, maximum bond/shear stress and slip values were experimentally measured and used in [6, 8] to propose new empirical formulas for such parameters, taking into account the influence of FRP stiffness. Failure modes were observed and curved fracture lines were detected in a number of specimens; hence the FRP deformation was found not to be constant along the transverse axis, showing a maximum in the middle of the bonded zone and a minimum at the edges of the FRP strip, as also reported in the following.

The modelled situation is depicted in Figure 2 (a), where the two prisms of concrete are connected through the FRP strip only; hence the strip is subjected to traction alone, whereas bending effects are negligible. Hence, such a schematisation exactly reproduces the situation in which a crack (or a series of cracks) is surrounded by unaltered concrete material (Figure 2 (b)); in this way the scope of the analyses is not to define and characterize the cracks' triggering and evolution but to simulate the concrete-FRP behaviour once a crack has started.

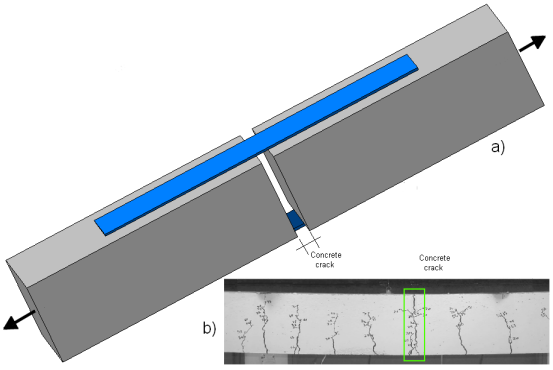

Figure 2: a) Test model, b) Real cracks pattern in a post-cracked beam.

These observations supported the need of developing an appropriate three-dimensional numerical modelling for a better understanding and simulation of the bond behaviour between FRP and

concrete. A similar approach has already been followed by e.g. [11] through a smeared-crack model, with the aim to catch the load-carrying capacity and failure behaviour of RC beams reinforced in flexure with a FRP sheet.

The typical double shear test has been reproduced through a 3D model; (one-eighth only is represented due to symmetry), the constitutive Drucker-Prager law is assumed for concrete elements, and for the FRP elements are assumed to behave in a linear-elastic manner, possibly undertaking large strains/displacements. Surface-to-surface contact conditions have been applied between FRP and adjacent concrete including the enhancement given by the strain-softening law according to the chosen scalar damage model. The procedure has been introduced to describe the coupled behaviour between concrete, FRP and adhesive resulting in specific bonding-debonding features under different load levels.

It is here briefly recalled that the delamination process is characterized by three states under continuous increase in the applied load level: in the first (state 1), cracks start in the FRP zone subjected to maximum shear: an increase in traction on the fibers induces an increase in shear stress at the concrete-FRP interface until the stress peak is reached and a micro-debonding occurs; as evidenced by (Figure 3), up to 40% of the maximum applied load (ML). In the second state the interface is subjected to both an increase in stress and softening (where a peak has already been reached), so that the stress peak moves from the cracks' triggering point towards the FRP's unloaded part causing a micro-debonding propagation. Under certain load levels (higher than 40%ML), the slip reaches its maximum value and stresses fall to zero, giving rise to the process of macro-debonding. The third state refers to complete debonding and the phenomenon eventually propagates in an instable manner: the final debonding depends on the cracking scheme characterizing the substratum (95%ML).

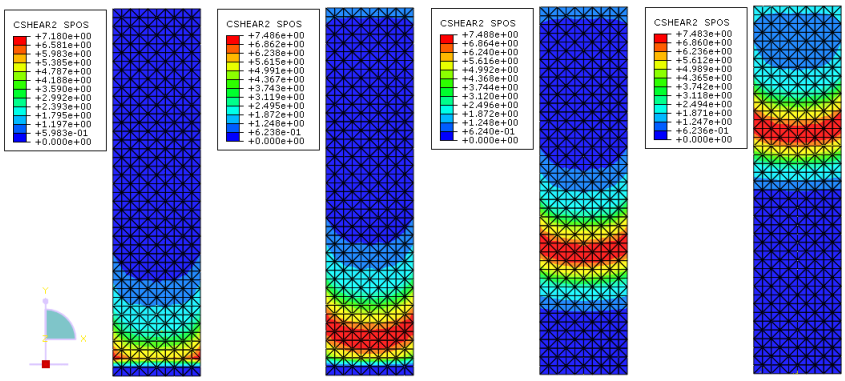

Figure 3: From left to right: contour maps of shear stress under 40%, 50%, 68%, 95% of the maximum load.

The stress distribution across the FRP plate follows a parabolic-type shape, in agreement with what obtained in the experimental tests [8]. The stress-strain relationship at the interface is typically an elastic-softening one, in agreement with the implemented damage law for the contact algorithm.

In the following the main numerical results are compared with the available experimental evidences; numerical shear stresses (Figure 4) decrease more rapidly along the fiber plate than the experimental ones but both the bonding length (the length along which the bond stress is not zero),

the curves' shapes and the peaks are respected. However it is to be said that experimentally strains only can be measured and corresponding stresses are calculated using a linear elastic theory, whereas numerical shear stresses take into account for nonlinear elasticity.

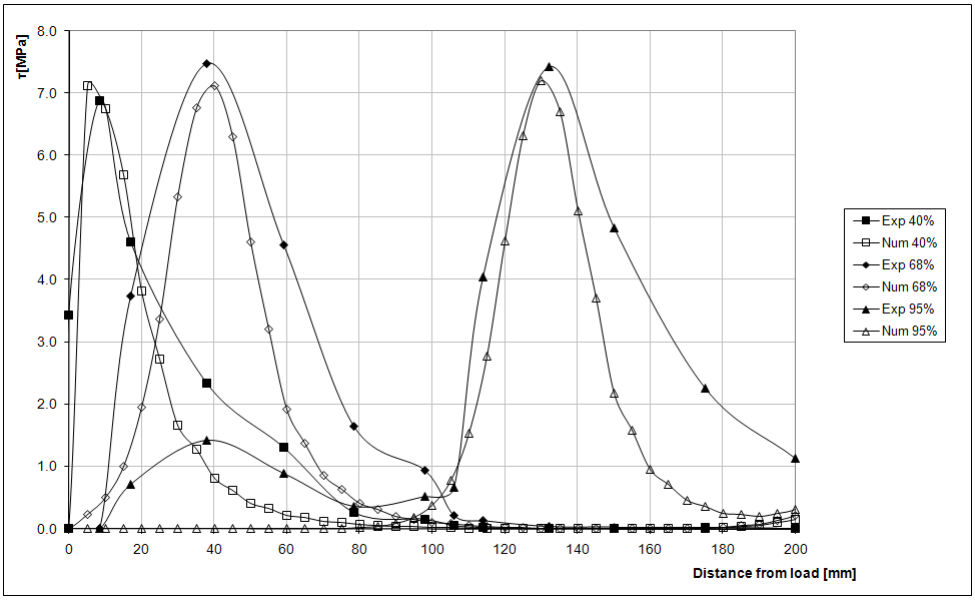

Figure 4: Numerical and experimental shear stresses along distance under 40%, 68% and 95% of the maximum applied load.

In Figure 5 the comparison between numerical and experimental slip curves is shown, slip calculated in agreement with [8],

$$s(x_i) = s(l_f) + \sum_{n=m} i\frac{1}{2}(\epsilon_{n-1} - \epsilon_n)(x_{n-1} - x_n) \tag{4}$$

starting from the values of the numerical strains and then performing a finite difference procedure.

It should be observed [5] that the experimental values of the axial strains of the FRP sheet, from which the experimental values of the bond stresses were obtained, were measured with closely spaced strain gauges. This method cannot produce accurate local bond-slip curves because the axial strains measured on the thin FRP plate generally show violent variations as a result of the discrete nature and the heterogeneity of concrete and the roughness of the underside of the debonded FRP sheet. The diagram shear stress versus slip (Figure 5) gives information on the fracture energy, being [6, 12, 13]:

$$G = \int_0^\infty \tau(s)ds \tag{5}$$

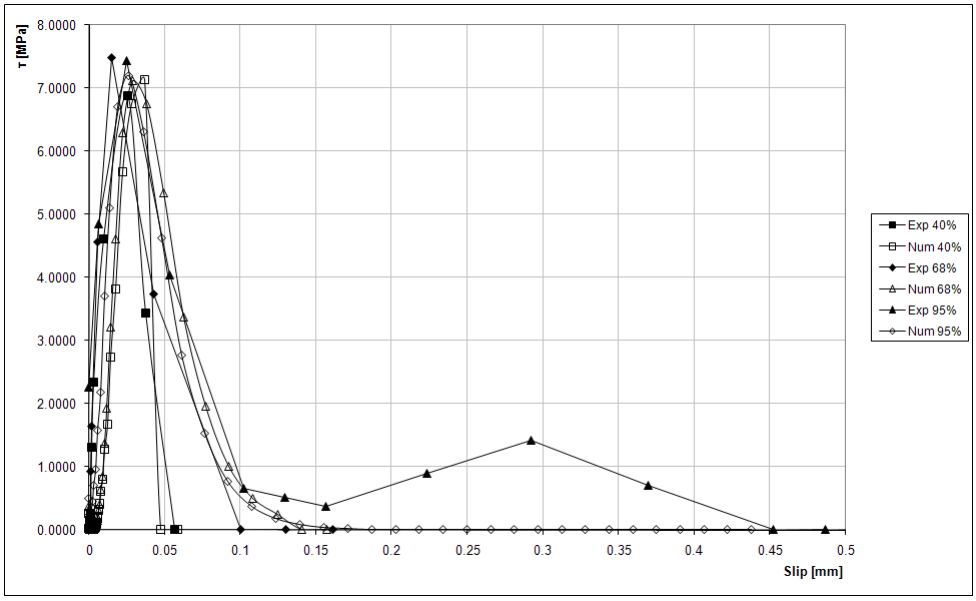

Figure 5: Shear stress versus slip under 40%, 68% and 95% of the maximum applied load.

Considering a discrete interval of data, the fracture energy takes the form

$$G_{II} = \sum_{i=1}^{n} \frac{\tau_{i+1} + \tau i}{2}(s_{i+1} - s_i) \tag{6}$$

Under a load level of 68%, when delamination starts, the fracture energy curve versus $\sum \Delta s_i = (s_{i+1} - s_i)$ has the shape depicted in (Figure 6 b), with reference to the shear stress-slip diagram (Figure 6 a); the typical S-shape of the work $G_{II}$of the shear tractions acting at the interface through the crack face displacements (when the energy release rates and mode decomposition approach is followed [7, 14, 15]) is reckoned, giving additional support to the proposed approach. Anyway, mixed modes as well as stiffness of the interface are not investigated here being out of scope of the present paper.

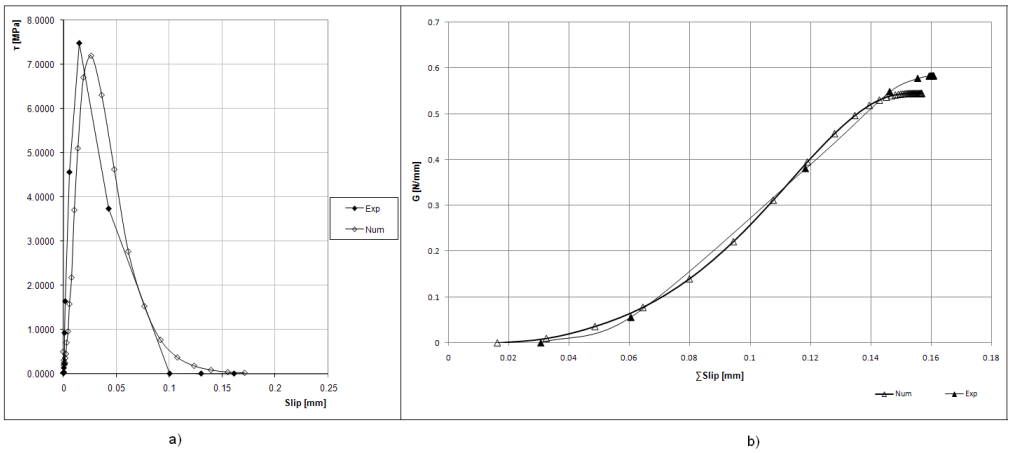

Figure 6: a) stress versus slip under 68% of the maximum applied load. b) Fracture energy curve under 68% of the maximum applied load.

As already discussed, such a 3D numerical model was additionally able to catch transversal effects during debonding, in agreement with the experimental results (Figure 7); particularly, the distribution of maximum strain across the interface follows the crack patches revealed after failure of the sample. By taking two reference control points (Figure 8 b), one in the middle and the other on the edge of the FRP strip, it is possible to evidence (Figure 8 a) that, under a fixed load level, the deformation at the middle position is sensibly higher than at the edge up to sample's collapse; again, during the loading process, the strain curves start diverging until a nearly instantaneous intersection, taking place at end analysis when the FRP has completely debonded.

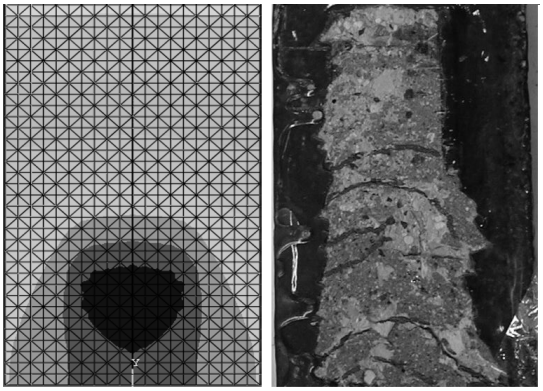

Figure 7: Numerical and experimental deformation/cracks distribution at the interface at debonding.

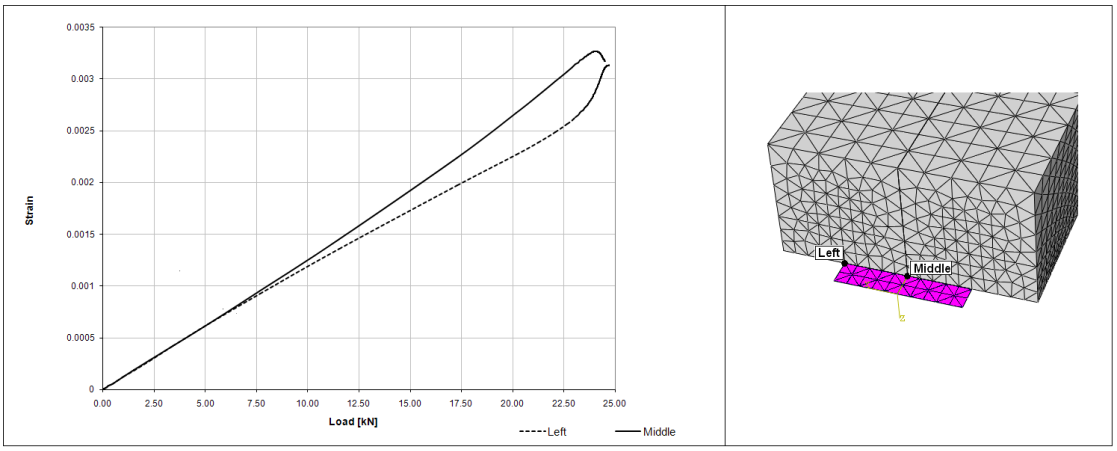

Figure 8: Strain histories of the control points.

This means that when using a 2D plane stress state approach, which necessarily assumes a constant stress distribution along the FRP width (not in agreement with experimental evidences), the stress resultants are overestimated; as already evidenced, the maximum stress difference between a middle and an edge point on the FRP is of about 12.5%, hence requiring an adjustment in the FRP's dimension assumed when performing 2D analyses. An equivalent FRP width could be obtained simply through equilibrium conditions for the shear stress resultants (Figure 9)

$$\int_0^B \tau ds = \tau_{max} B \tag{7}$$

$$B' = \frac{1}{\tau_{max}} \int_0^B \tau ds \tag{8}$$

The reduction in width is estimated as $B'/B = 7\%$

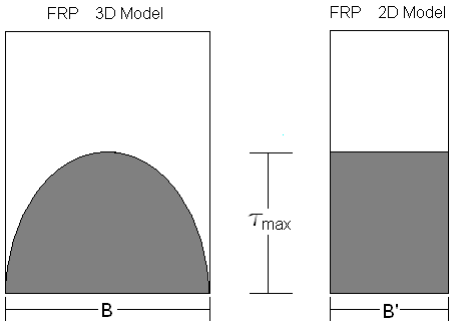

Figure 9: Integration scheme.

4 CONCLUSIONS

The bond behaviour between FRP and concrete elements has been here investigated, starting from available experimental results, through a calibrated and upgraded 3D mathematical-numerical model. The system has been proposed as composed by three different physical layers: the concrete base, the adhesive layer and the strengthening bonded FRP strip. The adhesion between layers has been modelled by means of an interface model whose elastic-damage constitutive law relates interlaminar stresses acting in the sliding direction. The F.E. ABAQUS code has been supplemented with a numerical procedure accounting for a scalar damage law inside the contact algorithm. Comparing the numerical results with those of a wide experimental investigation it has been shown by such 3D model that FRP deformation is not constant along the transversal axis but has a maximum in the middle of the bonded zone and a minimum at the edges of the FRP strips. This behaviour confirms experimental evidences and hence demonstrates the suitability of the proposed approach to capture the mechanism of debonding failure of FRP reinforcements and to catch transversal effects for developing a more realistic and comprehensive study of the delamination process.

References

[1] Pellegrino C., Modena C. “FRP shear strengthening of RC beams with transverse steel reinforcement," *J. Composites for Construction*, **6(2)**, 104-111 (2002).

[2] Pellegrino C, Modena C. “FRP shear strengthening of RC beams: experimental study and analytical modeling," *ACI Structural Journal*, **103 (5)**, 720-728 (2006).

[3] Pellegrino C, Modena C. “An experimentally based analytical model for shear capacity of FRP strengthened reinforced concrete beams," *Mechanics of Composite Materials*, **44(3)**, 231-244 (2008).

[4] Pellegrino, C., Modena C. “Flexural strengthening of real-scale RC and PRC beams with end-anchored pretensioned laminates," *ACI Structural Journal*, **106(3)**, (2009).

[5] Lu X Z, Teng J G, Ye L P, Jiang J J. “Bond-slip models for FRP sheets/plates bonded to concrete," *Engineering Structures* , **27**, 920-937 (2005).

[6] Savoia M, Ferracuti B, Mazzotti C. “Non Linear Bond-Slip law for FRP-Concrete Interface. FRPRCS-6 Conference," *Proceedings (K.H. Tan Ed.)*, Singapore 1-10 (2003).

[7] Bruno D, Greco F. “Mixed mode delamination in plates: a refined approach," *Int. J. Solids and Structures*, **38**, 9149-9177 (2001).

[8] Pellegrino C, Tinazzi D, Modena C. “Experimental Study on Bond Behaviour between Concrete and FRP Reinforcement," *ASCE J. Composites for Construction*, **12(2)**, 180-189 (2008).

[9] Mazars J, Pijaudier-Cabot G. “Continuum damage theory Ð application to concrete," *J. Engineering Mechanics*, **115 (2)**, 345-365. (1989).

[10] Majorana C E, Salomoni V, Schrefler B A. “Hygrothermal and mechanical model of concrete at high temperature," *Materials and Structures*, **31**, 378-386 (1998).

[11] Hormann M, Menrath H, Ramm E. “Numerical Investigation of Fiber Reinforced Polymers Poststrengthened Concrete Slabs," *J. Engineering Mechanics* , **128(5)**, 552 Ð 561(2002).

[12] Leung CKY, Asce M, Ng MYM, Luk H C Y. “Empirical Approach for Determining Ultimate FRP Strain in FRP-Strengthened Concrete Beams," *J. Composite for Construction*, **10(2)**, 125-138 (2006).

[13] Riccio A, Pietropaoli E. “Modeling Damage Propagation in Composite Plates with Embedded Delamination under Compressive Load," *J. Composite Materials*, **42**, 1309-1335 (2008).

[14] Point N, Sacco E. “A Delamination model for Laminated Composites. Int," *J. Solids Structures*, **33(4)**, 483-509 (1996).

[15] Bruno D, Greco F, Lonetti P. “A coupled interface-multilayer approach for mixed mode delamination and contact analysis in laminated composites," *Int. J. Solids and Structures*, **40**, 7245-7268 (2003).